

Lattice Boltzmann model for ultra-relativistic flows

F. Mohseni,^{1,*} M. Mendoza,^{1,†} S. Succi,^{2,‡} and H. J. Herrmann^{1,3,§}

¹ETH Zürich, Computational Physics for Engineering Materials,

Institute for Building Materials, Schafmattstrasse 6, HIF, CH-8093 Zürich (Switzerland)

²Istituto per le Applicazioni del Calcolo C.N.R., Via dei Taurini, 19 00185, Rome (Italy),
and Freiburg Institute for Advanced Studies, Albertstrasse, 19, D-79104, Freiburg, (Germany)

³Departamento de Física, Universidade Federal do Ceará,

Campus do Pici, 60455-760 Fortaleza, Ceará, (Brazil)

(Dated: February 6, 2013)

We develop a relativistic lattice Boltzmann model capable of describing relativistic fluid dynamics at ultra-high velocities, with Lorentz factors up to $\gamma \sim 10$. To this purpose, we first build a new lattice kinetic scheme by expanding the Maxwell-Jüttner distribution function in an orthogonal basis of polynomials and applying an appropriate quadrature, providing the discrete versions of the relativistic Boltzmann equation and the equilibrium distribution. To achieve ultra-high velocities, we include a flux limiter scheme, and introduce the bulk viscosity by a suitable extension of the discrete relativistic Boltzmann equation. The model is validated by performing simulations of shock waves in viscous quark-gluon plasmas and comparing with existing models, finding very good agreement. To the best of our knowledge, we for the first time successfully simulate viscous shock waves in the highly relativistic regime. Moreover, we show that our model can also be used for near-inviscid flows even at very high velocities. Finally, as an astrophysical application, we simulate a relativistic shock wave, generated by, say, a supernova explosion, colliding with a massive interstellar cloud, e.g. molecular gas.

PACS numbers: 47.11.-j, 02.40.-k, 95.30.Sf

I. INTRODUCTION

Relativistic fluid dynamics plays an important role in many contexts of astrophysics and high-energy physics, e.g. jets emerging from the core of galactic nuclei or gamma-ray bursts [1], shock induced Ritchmyer-Meshkov instabilities [2] and quark-gluon plasmas produced in heavy-ion collisions [3]. Hence, various numerical methods have been developed to study the relativistic hydrodynamics. Most of these methods are focussed on the solution of the corresponding relativistic macroscopic conservation equations. Among others, one can mention the methods based on second-order Lax-Wendroff scheme[4], smoothed particle hydrodynamics techniques [5, 6], Glimms (random choice) method [7] and high resolution shock-capturing methods [8]. Other methods, instead of solving the macroscopic equations, tackle the problem from the microscopic and mesoscopic points of view [9]. To this regard, the lattice Boltzmann (LB) method [10–12] a relatively new numerical approach, based on a minimal lattice version of the Boltzmann kinetic equation, has enjoyed increasing popularity for the last two decades. Within LB, representative particles stream and collide on the nodes of a regular lattice, with sufficient symmetry to reproduce the correct equations of macroscopic hydrodynamics. The main highlights of LB

are its computational simplicity, easy handling of complex geometries, and high amenability to parallel computing [13]. The LB method has met with remarkable success for the simulation of a broad variety of complex flows, from fully developed turbulence, all the way down to nanoscale flows of biological interest [14–16].

From a mathematical viewpoint, the standard lattice Boltzmann model can be obtained by expanding the equilibrium distribution, i.e. Maxwell-Boltzmann distribution, in a Hermite polynomials and using the nodes of polynomials, up to a certain order as the corresponding discretized velocities [17], using the Bhatnagar-Gross-Krook (BGK) approximation for the collision operator [18]. While the applications of the LB scheme cover an impressive array of complex fluid flows, its relativistic extension has been developed only in last few years [19, 20].

The relativistic LB (RLB) model was constructed by expanding the distribution function in powers of the fluid speed and finding the corresponding coefficients (Lagrange multipliers), by matching the moments of the Maxwell-Jüttner distribution in continuum velocity space. This model was shown capable of simulating weakly and moderately relativistic viscous flows, with $\beta = u/c \sim 0.3$, u being the typical flow speed. In particular, RLB was applied to the simulation of shock waves in quark-gluon plasmas, showing very good agreement with the results obtained by solving the full Boltzmann equation for multi-parton scattering (BAMPS), [21],

However, the aforementioned matching procedure does not provide a unique solution for the discrete equilibrium distribution function, satisfying the hydrodynamics moments of the Maxwell-Jüttner distribution. Moreover, the model lacks dissipation for the zero component

* mohsenif@ethz.ch

† mmendoza@ethz.ch

‡ succi@iac.cnr.it

§ hjherrmann@ethz.ch

of the energy-momentum tensor, and imposes a non-physical diffusion in the conservation of the number of particles [22]. These flaws, albeit very minor at moderate flow speeds, may become a concern for strongly relativistic flows. It is therefore highly desirable to develop more general and systematic approaches. To this purpose, let us observe that, due to the non-separability of the Maxwell-Jüttner distribution function into the three components of the momentum in Cartesian coordinates, its expansion in orthogonal polynomials is not as natural as in the classical case and some deliberation is required. For the fully relativistic regime, neglecting particle masses, and by using spherical coordinates, a lattice Boltzmann algorithm for the relativistic Boltzmann equation was developed in Ref. [23]. In this paper, the Maxwell-Jüttner distribution function was expanded in an orthogonal polynomials basis and discretized using a Gauss quadrature procedure. The model was based on the Anderson-Witting collision operator [24]. The results of simulating viscous quark-gluon plasma were compared to other hydrodynamic simulations and very good agreement was observed. However, using spherical coordinates makes the scheme incompatible with a cartesian lattice, and consequently, in the streaming procedure, a linear interpolation is required at each time step. Therefore, some crucial properties of the classical LB, e.g. exact streaming (zero numerical dispersion) and negative numerical diffusivity, are lost in the process.

In this paper, we develop a relativistic lattice Boltzmann model by expanding the Maxwell-Jüttner distribution in a set of orthogonal polynomials, and performing an appropriate quadrature in order to adjust the scheme to a D3Q19 (19 discrete velocities in three spatial dimensions) cell configuration [19, 20]. Moreover, we extend the model by using a minimum modulus flux limiter scheme and introducing the bulk viscosity term into the Boltzmann equation. We show that the model is numerically stable also at very high velocities, i.e. Lorentz factors up to $\gamma \sim 10$. Additionally, we show that this model can also be used to simulate near-inviscid flows, which corresponds to solve the Euler equation on the macroscopic level. This is well suited for astrophysical applications, where the viscosity is usually negligible. In fact, the astrophysical context presents possibly the richest arena for future applications of the present RLB scheme.

The paper is organized as follows: in Sec. II, the model description is presented in detail; and in Sec. III, several validations with other existing numerical models along with some results for shock waves in viscous quark-gluon plasmas and a 3D simulation of a shock wave colliding with a massive interstellar cloud are presented. Finally, in Sec. IV, a discussion about the model and the results is provided.

II. MODEL DESCRIPTION

We start the description of our model by writing the Maxwell-Jüttner equilibrium distribution function as

$$f^{\text{eq}} = A \exp(-p_\mu U^\mu / k_B T), \quad (1)$$

where, A is a normalization constant, k_B the Boltzmann constant, T the temperature and $(p^\mu) = (E/c, \mathbf{p})$ is the 4-momentum, with the energy of the particles E defined by

$$E = c p^0 = \frac{mc^2}{\sqrt{1 - u^2/c^2}}, \quad (2)$$

The macroscopic 4-velocity is $(U^\mu) = (c, \mathbf{u})\gamma(u)$, with \mathbf{u} the three-dimensional velocity, $\gamma(u) = 1/\sqrt{1 - u^2/c^2}$ the Lorentz's factor, m the mass, and c the speed of light. The relativistic Boltzmann equation, based on the Marle collision operator [25], reads as follows

$$p^\mu \partial_\mu f = -\frac{m}{\tau} (f - f^{\text{eq}}), \quad (3)$$

where f is the probability distribution function, and τ the single relaxation time. It is possible to write the Maxwell-Jüttner distribution in a simpler form by introducing the following change of variables:

$$\xi^\mu = \frac{p^\mu/m}{c_s}, \quad \chi^\mu = \frac{U^\mu}{c_s}, \quad (4)$$

$$c_s = \sqrt{\frac{k_B T}{m}}, \quad \nu = c/c_s, \quad (5)$$

and therefore, by replacing the new variables in Eq. (1) we have

$$f^{\text{eq}} = A \exp(-\xi_\mu \chi^\mu). \quad (6)$$

The temporal components, ξ^0 and χ^0 , can be calculated by the relations

$$\xi^0 = \sqrt{|\xi|^2 + \nu^2}, \quad (7)$$

$$\chi^0 = \nu \gamma(u), \quad \gamma(u) = \sqrt{1 + \frac{|\chi|^2}{\nu^2}}. \quad (8)$$

In analogy to the classical procedure of expanding the Maxwell-Boltzmann distribution in Hermite polynomials, we can also expand the Maxwell-Jüttner distribution, using orthogonal polynomials of the following form:

$$f^{\text{eq}}(\xi, \mathbf{x}, t) = w(\xi) \sum_{n=0}^{\infty} \frac{a_{(n)}(\mathbf{x}, t)}{N_{(n)}} F_{(n)}(\xi), \quad (9)$$

where

$$\int w(\xi) F_{(n)}(\xi) F_{(m)}(\xi) \frac{d^3 \xi}{\xi^0} = 0, \quad (10)$$

for $m \neq n$, and

$$N_{(n)} = \int w F_{(n)} F_{(n)} \frac{d^3 \xi}{\xi^0}. \quad (11)$$

To construct the appropriate orthogonal polynomials, we introduce the corresponding weight function as the equilibrium distribution at the local rest frame,

$$w(\xi) = A \exp(-\nu \xi^0). \quad (12)$$

Using the procedure proposed by Stewart [26], where the non-equilibrium distribution was expanded around the equilibrium, and the Maxwell-Jüttner distribution was used as the weight function to find the orthogonal polynomials, we can take up to second order,

$$F_{(0)} = 1, \quad (13)$$

and

$$F_{(1)}^\alpha = \xi^\alpha - a^\alpha, \quad (14)$$

$$F_{(2)}^{\alpha\beta} = \xi^\alpha \xi^\beta - a_\gamma^{\alpha\beta} F_{(1)}^\gamma - b^{\alpha\beta}, \quad (15)$$

where a^α , $a^{\alpha\beta}$ and $b^{\alpha\beta}$ are unknowns to be calculated using the Gram-Schmidt orthogonalization procedure

$$\begin{aligned} \int w F_{(0)} F_{(1)}^\alpha \frac{d^3 \xi}{\xi^0} &= \int w F_{(0)} F_{(2)}^{\alpha\beta} \frac{d^3 \xi}{\xi^0} \\ &= \int w F_{(1)}^\alpha F_{(2)}^{\alpha\beta} \frac{d^3 \xi}{\xi^0} = 0. \end{aligned} \quad (16)$$

The normalization coefficient for each polynomial is given by $\sqrt{N_{(n)}}$, and the coefficient $a_{(n)}$ is calculated using the relation

$$a_{(n)} = \int f^{\text{eq}} F_{(n)} \frac{d^3 \xi}{\xi^0}. \quad (17)$$

To calculate the coefficients a^α , $a^{\alpha\beta}$ and $b^{\alpha\beta}$, one needs the moments of the Maxwell-Jüttner distribution, which up to second order are given by [27]

$$\int f^{\text{eq}} \frac{d^3 \xi}{\xi^0} = 4\pi A K_1(\nu^2), \quad (18)$$

$$\int \xi^\alpha f^{\text{eq}} \frac{d^3 \xi}{\xi^0} = 4\pi A K_2(\nu^2) \chi^\alpha, \quad (19)$$

$$\int \xi^\alpha \xi^\beta f^{\text{eq}} \frac{d^3 \xi}{\xi^0} = -4\pi A (K_2(\nu^2) \eta^{\alpha\beta} - K_3(\nu^2) \chi^\alpha \chi^\beta), \quad (20)$$

where $K_n(\nu^2)$ is the modified Bessel function of the second kind of order n and $\eta^{\alpha\beta}$ is the Minkowski metric tensor with the signature $(+, -, -, -)$. The moments with respect to the weight function can be determined

by considering the above integrals in the local Lorentz rest frame.

For the sake of simplicity we define ϕ^α as

$$(\phi^\alpha) = (\chi^0, \mathbf{0}), \quad (21)$$

and by using the orthogonalization relations to calculate the unknowns, the resulting relativistic orthogonal polynomials are given by

$$F_{(0)} = 1, \quad (22)$$

$$F_{(1)}^\alpha = \xi^\alpha - \frac{K_2(\nu^2)}{K_1(\nu^2)} \phi^\alpha, \quad (23)$$

$$F_{(2)}^{\alpha\beta} = \xi^\alpha \xi^\beta - a_\gamma^{\alpha\beta} F_{(1)}^\gamma - b^{\alpha\beta}, \quad (24)$$

where

$$b^{\alpha\beta} = \frac{K_3(\nu^2)}{K_1(\nu^2)} \phi^{\alpha\beta} - \frac{K_2(\nu^2)}{K_1(\nu^2)} \eta^{\alpha\beta}, \quad (25)$$

and

$$\begin{aligned} a_\gamma^{\alpha\beta} &= \frac{\eta_{\gamma\delta} + D(\nu) \phi_\gamma \phi_\delta}{2K_2(\nu^2)D(\nu)} \left[K_3(\nu^2) (\eta^{\alpha\delta} \phi^\beta + \eta^{\beta\delta} \phi^\alpha) \right. \\ &\quad - \left(K_3(\nu^2) - \frac{[K_2(\nu^2)]^2}{K_1(\nu^2)} \right) \eta^{\alpha\beta} \phi^\delta \\ &\quad \left. + \left(K_4(\nu^2) - \frac{K_2(\nu^2) K_3(\nu^2)}{K_1(\nu^2)} \right) \phi^\alpha \phi^\beta \phi^\delta \right]. \end{aligned} \quad (26)$$

Here, the function $D(\nu)$ is defined by

$$[1 + D(\nu)]^{-1} = 1 + \frac{K_2(\nu^2)}{K_1(\nu^2)} - \frac{K_3(\nu^2)}{K_2(\nu^2)}. \quad (27)$$

By following this procedure, we can calculate higher order polynomials. However, since in this work we are interested in recovering only up to the second moment of the Maxwell-Jüttner distribution (energy-momentum tensor), using the expansion up to the second order is sufficient. In particular, the third, fourth and fifth order moments, which are needed to describe highly viscous fluids, would increase dramatically the complexity of our expansion, and consequently its numerical implementation. This is a very interesting subject for future extensions of this work.

Additionally, in the ultrarelativistic limit, where $k_B T \gg mc^2$, i.e. $\nu \ll 1$, we can use the following asymptotic relation:

$$\lim_{\nu \rightarrow 0} K_n(\nu^2) = \frac{2^{n-1} (n-1)!}{\nu^{2n}}. \quad (28)$$

Using the resulting polynomials $F_{(n)}$, coefficients $a_{(n)}$ and $N_{(n)}$ with Eqs. (9) and (28) we can expand the Maxwell-Jüttner distribution in orthogonal polynomials,

$$\begin{aligned} f^{\text{eq}} &\simeq A e^{-\nu \xi^0} \left\{ 1 + \left(\frac{\chi^0 \xi^0 + 3}{2} - \frac{\chi^0}{\nu} - \frac{\xi^0 \nu}{4} \right) (\boldsymbol{\xi} \cdot \boldsymbol{\chi}) \right. \\ &\quad + \xi^x \xi^y \chi^x \chi^y + \xi^x \xi^z \chi^x \chi^z + \xi^y \xi^z \chi^y \chi^z \\ &\quad \left. + \frac{4}{\nu^4 - 6\nu^2 - 15} [(\xi^x)^2 (\chi^x)^2 + (\xi^y)^2 (\chi^y)^2 + (\xi^z)^2 (\chi^z)^2 \right. \\ &\quad \left. + \left(\frac{1-\nu^2}{\nu} \xi^0 - \frac{4-2\nu^2}{\nu^2} \right) (\boldsymbol{\chi} \cdot \boldsymbol{\chi})] \right\}, \end{aligned} \quad (29)$$

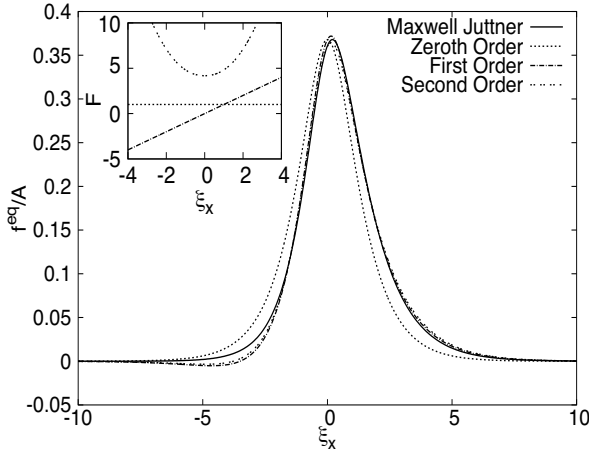


FIG. 1. Comparison between the Maxwell Jüttner distribution function and the zeroth, first and second order expansions in one space dimension for $\beta = 0.2$. In the inset, $F_{(0)}$, $F_{(1)}$ and $F_{(2)}$ polynomials, in the local rest frame are shown.

up to second order and in the ultrarelativistic regime.

One can compare the Maxwell Jüttner distribution with the zeroth, first and second order expansions in the one dimensional case. The result of the distributions versus ξ_x for the case $\beta = |\mathbf{u}|/c = 0.2$ is presented in Fig. 1. Here, we can observe that, as expected, as the order of the expansion increases, the expansion becomes more accurate. Note that the expanded distributions become negative for values of ξ_x , around -3 . However, this is of no concern for our model since, as we shall see shortly, the quadrature requires only $\xi_x \sim 1$. For illustrative purposes, in the inset of Fig. 1, we show, for $\nu = 1$ and in the local rest frame, the polynomials corresponding to the zeroth ($F_{(0)}$), first ($F_{(1)}$), and second ($F_{(2)}$) orders.

We can write the Boltzmann equation, Eq.(3), as follows:

$$\xi^0 \partial_t f + \xi^a \partial_a f = -\frac{\nu}{\tau c} (f - f^{\text{eq}}), \quad (30)$$

where latin subscript a runs over the spatial coordinates. In order to discretize Eq.(30) and avoid a multi-time lattice, we need to consider the temporal components of the discretized velocity 4-vector, i.e. ξ_i^0 , as constant. Therefore, a transformation of the temporal component of both ξ^α and χ^α is required. We can write $(\xi^\alpha) = (c_t/c_0, \mathbf{c}_a)$ and $(\chi^\alpha) = (\chi^0/c_0, \boldsymbol{\chi})$, where c_t , c_0 and \mathbf{c}_a are constants related to the size of the lattice. We will use a lattice configuration D3Q19 (19 discrete vectors in 3 spatial dimensions), which can be expressed as

$$\mathbf{c}_a = \begin{cases} (0, 0, 0) & i = 0; \\ c_a (\pm 1, 0, 0)_{FS} & 1 \leq i \leq 6; \\ c_a (\pm 1, \pm 1, 0)_{FS} & 7 \leq i \leq 18, \end{cases} \quad (31)$$

where the subscript FS denotes a fully symmetric set of points.

To find the discretized weights for the lattice, we use a quadrature procedure. According to the quadrature rule, the discretized weights should satisfy the relation

$$\int R(\xi) w(\xi) \frac{d^3 \xi}{\xi^0} = \sum_{i=1}^N R(\xi_i) w_i, \quad (32)$$

where $R(\xi)$ is an arbitrary polynomial of order $2N$ or less. Using this relation, we can construct a system of equations by replacing $R(\xi)$ with different combinations of zeroth, first and second order polynomials. The left hand side of the above equation can be calculated by using Eq.(18) to (20). Thus, the resulting discrete weights are given by

$$w_0 = 1 + \frac{4c_t^2 \nu^2}{361c_0^2} - \frac{c_t^2}{c_a^2 c_0^2}, \quad (33)$$

$$w_i = \frac{c_t^2}{2166c_0^2 c_a^2} (361 - 8c_a^2 \nu^2), \quad (34)$$

for $1 \leq i \leq 6$, and

$$w_i = \frac{c_t^2 \nu^2}{1083c_0^2}, \quad (35)$$

for $7 \leq i \leq 18$. Note that we still need to calculate the constants related to the size of the lattice, i.e. c_a , c_t and c_0 .

The discretized 4-momenta should satisfy the following relation for the energy-momentum tensor, i.e. the second order moment of the distribution function,

$$\int p^\alpha p^\beta f^{\text{eq}} \frac{d^3 p}{p^0} = \sum_{i=1}^N p_i^\alpha p_i^\beta f_i^{\text{eq}} \\ = (\epsilon + p) \frac{U^\alpha U^\beta}{c^2} - p \eta^{\alpha\beta} = T_{\text{eq}}^{\alpha\beta}, \quad (36)$$

where p is the hydrostatic pressure, ϵ the energy density and $T_{\text{eq}}^{\alpha\beta}$ denotes the energy-momentum tensor at equilibrium. Note that higher order moments of the discrete equilibrium distribution can be calculated by performing the respective sums $T^{\alpha\beta\cdots\gamma} = \sum_{i=1}^N p_i^\alpha p_i^\beta \cdots p_i^\gamma f_i^{\text{eq}}$. However, they would not correspond to the ones of the Maxwell-Jüttner distribution, because the latter require an expansion in higher order polynomials. Their contribution to the dynamics of the fluid become important at high values of the Knudsen number (high momentum diffusivity), and since they are not exactly recovered, our model does not work properly in that regime. Fortunately, many applications in astrophysics and high energy physics deal with near-inviscid or weakly viscous fluids.

We can simply find the constants related to the lattice size, using the fact that in the tensor, the coefficient of $U^\alpha U^\beta$ for different α and β should be always the same. The calculated values for the constants are

$$c_a = \frac{\sqrt{19}}{\nu}, \quad c_t/c_0 = \frac{\sqrt{27}}{\nu}, \quad c_0 = \frac{3}{8}(9 - 2\sqrt{3}). \quad (37)$$

In the ultrarelativistic limit and considering the natural units $c = k_B = 1$, from the energy-momentum tensor, one can obtain the following relations:

$$\epsilon + p = \frac{4n}{\nu^2}, \quad p = \frac{n}{\nu^2}, \quad \epsilon = 3p, \quad (38)$$

finding that the relation between ϵ and p corresponds to the well-known state equation in the ultrarelativistic limit.

Note that due to the fact that we have supposed ξ_i^0 to be constant, to avoid a multi-time evolution lattice, there are some equations in the quadrature procedure for the first order moment and the second order moment of the distribution function which could not be satisfied simultaneously. Indeed, we can choose whether to recover the first order moment or the second order moment in the quadrature. To satisfy the first moment of the Maxwell-Jüttner distribution function leads to recover the equation for the conservation of number of particles, $\partial_\alpha N^\alpha = 0$, and the second order moment, the equation for the conservation of momentum-energy, $\partial_\alpha T^{\alpha\beta} = 0$. To calculate the four unknowns, namely U^x, U^y, U^z and ϵ , the four equations corresponding to T^{00}, T^{0x}, T^{0y} and T^{0z} components of the energy-momentum tensor and equation of state $\epsilon = 3p$ would be enough. Therefore, by using the ultrarelativistic equation of state the dynamics of the system is not affected by the number of particles and the equation for the conservation of momentum-energy is therefore sufficient to describe the entire dynamics of the relativistic fluid. For this reason, our quadrature is targeted to recover the second order moment, using a separate distribution function to recover the equation for the conservation of number of particles, $\partial_\alpha N^\alpha = 0$, based on the model proposed by Hupp et al. [28].

Using the mentioned lattice to discretize the Boltzmann equation, Eq.(30) can be written as follows:

$$f_i(\mathbf{x} + \mathbf{c}_a \frac{c_0}{c_t} \delta t, t + \delta t) - f_i(\mathbf{x}, t) = -\frac{c_0 \nu \delta t}{\tau c_t} (f_i - f_i^{\text{eq}}). \quad (39)$$

The left hand side of the equation is readily recognized as free-streaming, while the right hand side is the discrete version of the collision operator according to the model of Marle. In this equation, the following relation between δt and δx has been used:

$$\delta t = \frac{c_t \delta x}{c_a c_0}. \quad (40)$$

In the ultra-relativistic limit, the shear viscosity using the model of Marle can be calculated as:

$$\eta = \frac{(\epsilon + p)}{\nu^2} \left(\tau - \frac{1}{2} \right). \quad (41)$$

In our model, this expression is only valid for small values of τ (which leads to small values of the Knudsen number), where higher order moments of the distribution can be neglected.

At each time step and at each lattice point, the values of the macroscopic velocity and energy density can be evaluated using the energy-momentum tensor as mentioned previously.

A. Extended model for high velocities

At high velocities ($\beta > 0.6$), due to the compressibility effects (high Mach numbers), the described numerical scheme shows artificial discontinuities in the velocity and pressure profiles, leading to numerical instabilities in the long-term evolution. We shall return to this issue in Sec. III. The relativistic Mach number can be expressed as $M^R = \gamma(u)|\mathbf{u}|/\gamma(c_{so})c_{so}$ where c_{so} is the velocity of sound, which is $c_{so} = c/\sqrt{3}$ in the ultra-relativistic regime. In order to overcome this problem, we first use a modified version of the D3Q19 cell configuration, which is denoted by $(\xi_i^\alpha) = (c_t/c_0, \mathbf{c}_a)$, where \mathbf{c}_a takes now the following form:

$$\mathbf{c}_a = \begin{cases} (0, 0, 0) & i = 0; \\ c_a(\pm 1, 0, 0)_{FS} & 1 \leq i \leq 6; \\ 2c_a(\pm 1, \pm 1, 0)_{FS} & 7 \leq i \leq 18. \end{cases} \quad (42)$$

Since some of the discrete velocities go beyond first and second neighbors in the lattice, the scheme can support higher flow speeds. In order to find the discretized weights, as well as the size of the lattice cells, we repeat the same procedure as before obtaining

$$w_0 = 1 + \frac{7c_t^2 \nu^2}{676c_0^2} - \frac{c_t^2}{c_a^2 c_0^2}, \quad (43)$$

$$w_i = \frac{c_t^2}{1014c_0^2 c_a^2} (169 - 2c_a^2 \nu^2), \quad (44)$$

for $1 \leq i \leq 6$,

$$w_i = \frac{c_t^2 \nu^2}{8112c_0^2}, \quad (45)$$

for $7 \leq i \leq 18$, and

$$c_a = \frac{\sqrt{13}}{\nu}, \quad c_t/c_0 = \frac{\sqrt{27}}{\nu}, \quad c_0 = \frac{3}{8}(9 - 2\sqrt{3}). \quad (46)$$

The second step to extend our model, is to introduce the minimum modulus (min mod) scheme to discretize the spatial components in the streaming term in the Boltzmann equation, Eq.(30), i.e. $p_i^a \partial_a f_i$. The min mod scheme is a flux limiter method that efficiently reduces the instability especially when step discontinuities occur (e.g. in shock waves). The following relations characterize this scheme [29]:

$$\partial_a(p_i^a f_i) = \frac{1}{|\delta x \mathbf{e}_a|} [h_i^a(\mathbf{x} + \delta x \mathbf{e}_a) - h_i^a(\mathbf{x})], \quad (47)$$

$$h_i^a(\mathbf{x}) = f_i^{a^L}(\mathbf{x}) + f_i^{a^R}(\mathbf{x}), \quad (48)$$

$$f_i^{a^L}(\mathbf{x}) = f_i^{a^+}(\mathbf{x}) + \frac{1}{2} \min \text{mod} \left(\Delta f_i^{a^+}(\mathbf{x}), \Delta f_i^{a^+}(\mathbf{x} - \delta x \mathbf{e}_a) \right), \quad (49)$$

$$f_i^{a^R}(\mathbf{x}) = f_i^{a^-}(\mathbf{x} + \delta x \mathbf{e}_a) - \frac{1}{2} \min \text{mod} \left(\Delta f_i^{a^+}(\mathbf{x}), \Delta f_i^{a^+}(\mathbf{x} + \delta x \mathbf{e}_a) \right), \quad (50)$$

$$f_i^{a^+} = \frac{1}{2}(p_i^a + |p_i^a|)f_i, \quad f_i^{a^-} = \frac{1}{2}(p_i^a - |p_i^a|)f_i, \quad (51)$$

$$\Delta f_i^{a^\pm}(\mathbf{x}) = f_i^{a^\pm}(\mathbf{x} + \delta x \mathbf{e}_a) - f_i^{a^\pm}(\mathbf{x}), \quad (52)$$

where \mathbf{e}_a is a unit vector in the direction of the corresponding spatial coordinate. Let us remind that p_i^a is independent of spatial coordinates. The min mod function is defined as

$$\min \text{mod}(X, Y) = \frac{1}{2} \min(|X|, |Y|) \times [\text{Sign}(X) + \text{Sign}(Y)]. \quad (53)$$

Note that in classical flows, the bulk viscosity plays an important role in highly compressible flows and enhances the stability of numerical simulations of fluids at very high velocities, including shock waves [30]. However, in the ultrarelativistic limit, the energy-momentum tensor is traceless and the bulk viscosity is zero [31, 32]. Therefore, in order to include the bulk viscosity, we add the following term to the right hand side of the Boltzmann equation, Eq.(30):

$$\lambda_i \sum_{a=x,y,z} \partial_a^2 f_i, \quad (54)$$

where

$$\lambda_i = \begin{cases} 0 & i = 0; \\ \alpha \delta x & i \neq 0, \end{cases} \quad (55)$$

where α is a constant. A central finite difference scheme is used to calculate the second order derivative. Chapman-Enskog analysis reveals that the bulk viscosity obtained by this extra-term takes the form

$$\eta_b = \frac{4p\alpha\nu^6}{27}. \quad (56)$$

Note that, like the analytical expression of the bulk viscosity for the model of Marle, the above-mentioned bulk viscosity is also proportional to T^{-3} , and as expected goes to zero in the ultra-relativistic limit $\nu \rightarrow 0$. However, this small value of bulk viscosity is sufficient to stabilize the system at high velocities, as we are going to show in the next section.

Once all of the extensions above are taken into account, the discretized form of the relativistic Boltzmann equation takes the following expression:

$$\begin{aligned} & f_i(\mathbf{x}, t + \delta t) - f_i(\mathbf{x}, t) \\ & + \frac{c_0}{c_t} \frac{\delta t}{\delta x} [h_i^a(\mathbf{x} + \delta x \mathbf{e}_a) - h_i^a(\mathbf{x})] = \\ & - \frac{c_0 \nu \delta t}{\tau c_t} [f_i(\mathbf{x}, t + \delta t) - (2f_i^{\text{eq}}(\mathbf{x}, t) - f_i^{\text{eq}}(\mathbf{x}, t - \delta t))] \\ & + \frac{c_0 \nu \delta t}{c_t} \lambda_i \sum \partial_a^2 f_i(\mathbf{x}, t), \end{aligned} \quad (57)$$

where an implicit representation of the collision term is used, as proposed in Ref. [33] to enhance the stability of the collision term.

As mentioned above, for the cases where the dynamics of the number of particles density is also needed, one has to solve the conservation equation, i.e. $\partial_\alpha N^\alpha = 0$, with $N^\alpha = nU^\alpha$. For this purpose, we add an extra distribution function, h_i , based on the model proposed by Hupp et al. [28], which follows the dynamics of the Boltzmann equation given by Eq. (57), without the λ_i coefficient term. The corresponding modified equilibrium distribution function is given by:

$$h_i^{\text{eq}} = w_i' n \gamma(u) \left(\frac{c_0}{c_t} + 3(\mathbf{c}_a \cdot \mathbf{u}) + \frac{9}{2}(\mathbf{c}_a \cdot \mathbf{u})^2 - \frac{3}{2}|\mathbf{u}|^2 \right), \quad (58)$$

$$w_0' = \frac{1}{10}, \quad w_i' = \frac{6}{35} - \frac{1}{42c_a^2}, \quad (59)$$

for $1 \leq i \leq 6$,

$$w_i' = \frac{1}{84c_a^2} - \frac{3}{280} \quad (60)$$

for $7 \leq i \leq 18$, where we have used our new cell configuration, and w_i' are the respective discrete weights.

Having discussed the model, we move on to the next section, where different validations and results for the Riemann problem are provided, along with a simulation of a shock wave colliding with a interstellar cloud.

III. VALIDATION AND RESULTS

In order to validate the model and the numerical procedure, we present results for the simulation of relativistic shock wave propagation in viscous quark-gluon plasma. The associated Riemann problem is studied and several comparisons are drawn between the present RLB model and the existing literature. Indeed, the Riemann problem is a challenging test for numerical methods, since it involves a shock and rarefaction wave.

The initial condition of the Riemann problem consists of two regions with different pressure, which are separated by a membrane in the middle of the interval. The pressure in the left region (P_0) is higher than the pressure in the right region (P_1). Both sides of the discontinuity are supposed to be initially in the rest frame. Hence, spatial components of initial velocities for both sides are set

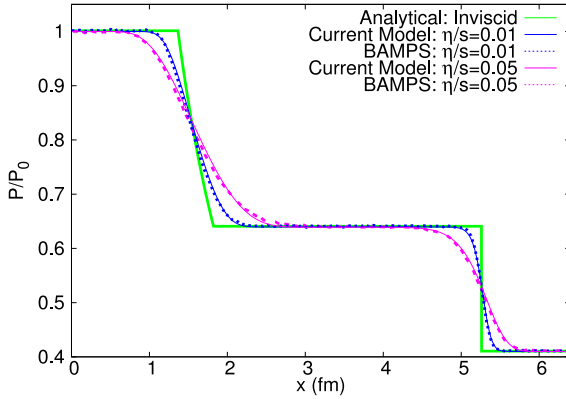


FIG. 2. Comparison of the velocity profile of the current model and BAMPS, for different values of η/s at weakly relativistic regime.

to zero. At time $t = 0$, the membrane is removed and a shock wave propagates from the high pressure region into the low pressure region with velocity v_{shock} and a rarefaction wave propagates in the opposite direction. The shock velocity only depends on the pressure difference, the equation of state, and can be calculated analytically [34, 35]. The region between the shock wave and the rarefaction wave has a constant pressure, corresponding to the so-called shock plateau. In this region the velocity is also constant (v_{plat}).

In order to compare our results with existing models, we use the same conditions as in Ref. [19, 21]. Therefore, one dimensional simulations are carried out using $800 \times 1 \times 1$ cells, where open boundary conditions are considered at the two ends. The cell size δ_x is taken to be unity, which corresponds to $\delta_x = 0.008 \text{ fm}$ in IS units and δ_t can be calculated from Eq.(40). We use η/s as the characteristic parameter of shear viscosity, where the viscosity is defined in Eq.(41) and the entropy density is given by $s = 4n - n \ln \lambda$, with $\lambda = n/n^{eq}$ being the fugacity of gluons, $n^{eq} = d_G T^3 / \pi^2$ the equilibrium density, and $d_G = 16$ the degeneracy of gluon.

For the first validation test, we set the initial pressure at the left and right sides to $P_0 = 5.43 \text{ GeV/fm}^3$ and $P_1 = 2.22 \text{ GeV/fm}^3$, respectively. This corresponds to 2.495×10^{-7} and 1.023×10^{-7} in numerical units, respectively. Fig. 2 shows the pressure profiles at time $t = 3.2 \text{ fm/s}$ for different values of η/s , compared to the results reported by Ref. [21] (hereafter BAMPS) and an analytical solution for the inviscid case reported in Ref. [34]. As one can notice, very satisfactory agreement for different values of η/s is obtained..

As mentioned previously, the lattice Boltzmann method is computationally very efficient. For instance, the above simulation took ~ 220 ms on a standard PC, which is approximately an order of magnitude faster than corresponding hydrodynamic simulations. To further elaborate on the validity of our model, we compare with the results of Ref. [19] (hereafter previous LBS) for

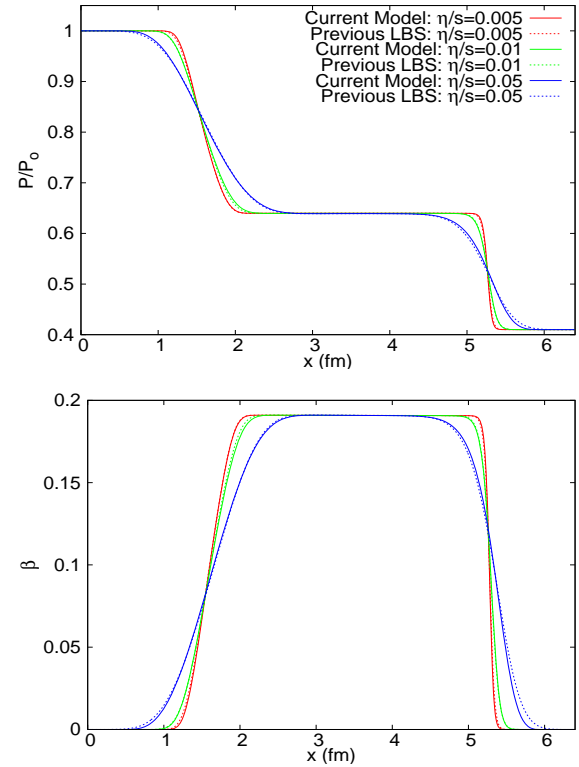


FIG. 3. Comparison between the current model and the previous LBS model at different η/s , for the pressure (top) and velocity (bottom) profiles in the weakly relativistic regime.

different values of η/s . Fig. 3 shows that pressure and velocity profiles are in good agreement with previous LBS simulations. It is worth mentioning that, as it is apparent from Fig. 3, the above mentioned pressure difference corresponds to $\beta = |v_{\text{plat}}| \sim 0.2$ (weakly relativistic regime), while the velocity of the shock is $v_{\text{shock}} \sim 0.65$.

To study higher velocities, we consider higher pressure difference between the left side and the right side, namely $P_0 = 5.43 \text{ GeV/fm}^3$ and $P_1 = 0.339 \text{ GeV/fm}^3$. This corresponds to 2.495×10^{-7} and 1.557×10^{-8} in numerical units, respectively. The resulting pressure and velocity profiles for $\eta/s = 0.01$, are compared to the results with previous LBS in Fig. 4, showing again very good agreement. It should be noted that, due to the above-mentioned pressure difference, the matter behind the shock moves with the velocity $\beta \sim 0.6$ (moderately relativistic regime), while the shock itself goes with the velocity $v_{\text{shock}} \sim 0.92$.

Note that the proposed model in the non-extended form (hereafter basic model) becomes numerically unstable for higher velocities ($\beta > 0.6$). This instability is due to compressibility effects. It is known that the lattice Boltzmann method is intrinsically suited to low Mach number flows (low compressibility effects). Therefore, in order to overcome this problem, we use our extended model, which enhances the stability of the nu-

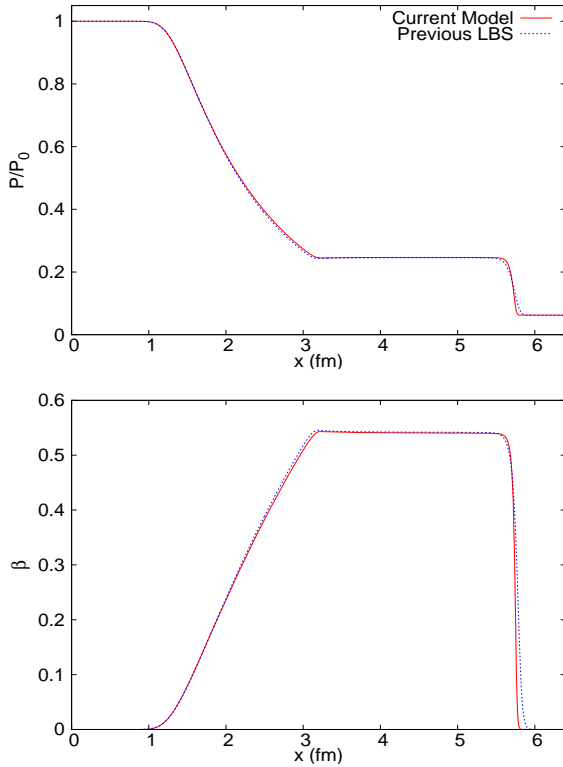


FIG. 4. Comparison between the current model and the previous LBS model at $\eta/s = 0.01$, for the pressure (top) and velocity (bottom) profiles in the moderately relativistic regime.

merical procedure without any appreciable loss of computational efficiency. To further investigate this issue, we carry out two simulations with the same conditions for relatively higher velocity, one using the basic model, and the other one using the extended one. The pressure is set to be $P_0 = 5.43\text{GeV}/\text{fm}^3$ and $P_1 = 0.1695\text{GeV}/\text{fm}^3$ for the left side and the right side, respectively, which corresponds to 2.495×10^{-7} and 7.785×10^{-9} in numerical units. Here, $\eta/s = 0.01$, $\delta_t/\delta_x = 0.25$, and $\alpha = 0.15$ for the extended model.

The results for the pressure and velocity profiles are shown in Fig. 5 at time $t = 3.2\text{fm}/s$. Note that the applied pressure difference corresponds to $\beta \sim 0.7$. Using the basic model, an artificial discontinuity is observed in both the pressure and velocity profiles, which is due to instability problems in the numerical scheme. However, the extended model proves capable of handling the simulation, the problem of the artificial discontinuity being solved completely. Additionally, apart from the region affected by the discontinuity, the good agreement between the results of two models can be interpreted as a validation for the precision of the extended model. The required CPU time for the simulation using the extended model and for the chosen value of δ_t/δ_x is 1069 ms.

To the best of our knowledge, to date, there was no reported simulation of shock wave in viscous flow for

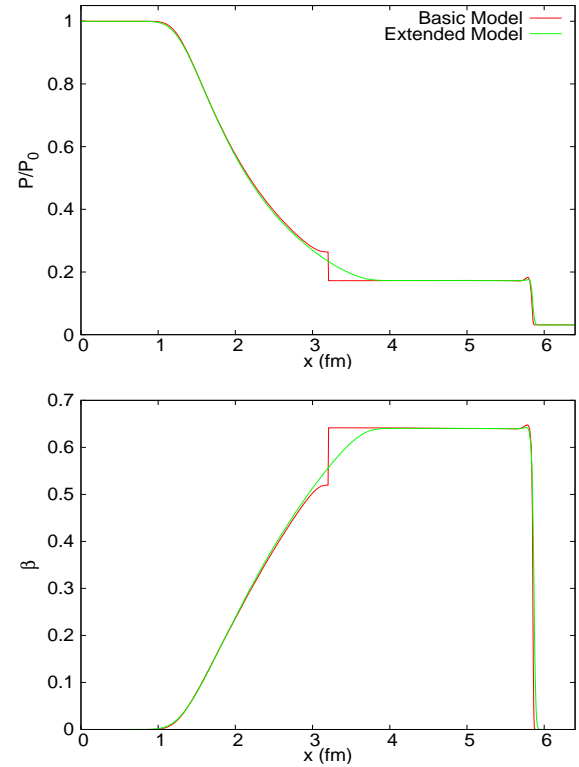


FIG. 5. Comparison between the basic and extended models for the pressure (top) and velocity (bottom) profiles in the moderately relativistic regime.

$\beta > 0.6$. However, for the inviscid case, which corresponds to the Euler equation at macroscopic scale, there exists an analytical solution for the Riemann problem. Therefore, in order to validate our extended model, we compare our results with the analytical solution of the inviscid case in Ref. [35]. Hence, we need to solve the Euler equation by ignoring the viscous effects. It is worth mentioning that, in the classical lattice Boltzmann method, the numerical solution becomes unstable as one tries to set the shear viscosity to zero ($\tau = 1/2$). This is also the case for our basic model. However, in the extended model we can solve the Euler equation by changing the collision step, such that instead of implementing the regular collision, we simply set the discretized distribution functions to their corresponding equilibrium values. This is similar to the procedure used in Ref.[36] to solve Euler equation in the non-relativistic case. As one can notice from the Boltzmann equation, this corresponds to ignore the non-equilibrium part of the distribution function which contains the information about the dissipation. Therefore, we neglect the viscous effects in the macroscopic equations, obtaining the Euler equations.

The results of our inviscid simulation are compared to the analytical results in Fig. 6. To drive the shock at velocity $\beta \sim 0.9$ (highly relativistic regime), the applied pressure is set to $P_0 = 5.43\text{GeV}/\text{fm}^3$ and $P_1 =$

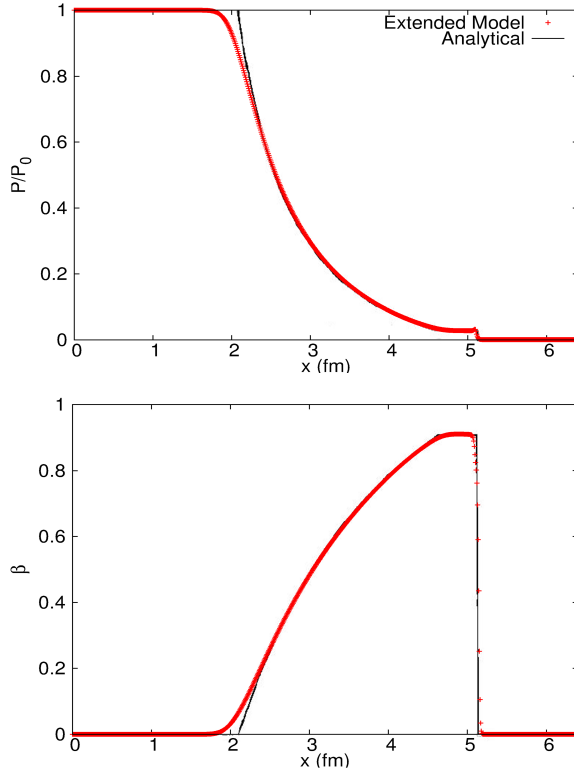


FIG. 6. Comparison between the extended model and analytical results for the pressure (top) and velocity (bottom) profiles in the highly relativistic regime.

$5.43 MeV/fm^3$, which corresponds to 2.495×10^{-7} and 2.495×10^{-10} in numerical units, respectively. The results are shown at $t = 2.0 fm/s$ and very good agreement is found. The small discrepancies between our simulation and the analytical curve are related to the fact that a small value of bulk viscosity inevitably remains in our simulation, due to the λ_i coefficients, which are needed to increase the stability of the model. This issue makes a subject for future investigations. The CPU time required for the simulation shown in Fig. 6 is 593 ms.

The fact that we can model properly the Euler equation at very high velocities opens the possibility of using our model in astrophysical applications, where velocities are usually high and viscous effects are negligible.

Fig. 7 shows the same result at $\beta \sim 0.9$ for different viscosities, compared to the inviscid case at $t = 2.0 fm/s$. The same conditions as mentioned above are considered again. The effects of increasing η/s at this velocity are similar to the case of lower velocity.

In order to demonstrate the ability of the model to simulate ultra-high velocities, we consider the case of the initial pressures $P_0 = 5.43 GeV/fm^3$ and $P_1 = 0.0543 MeV/fm^3$ which corresponds to 2.495×10^{-7} and 2.495×10^{-12} in numerical units, respectively. We set $\delta_t/\delta_x = 0.25$, $\alpha = 0.2$, and $\eta/s = 0.01$. The results for the velocity profile and local Lorentz's factor

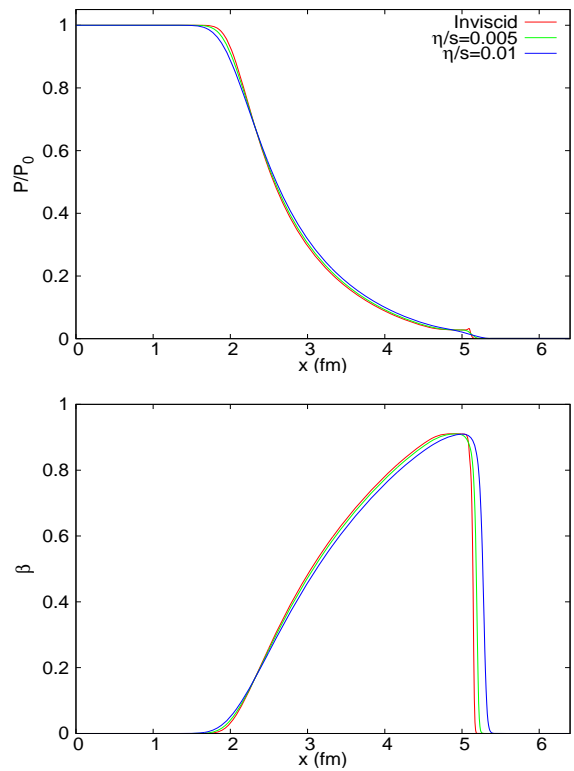


FIG. 7. Comparison of the results for the inviscid case and different η/s , for the pressure (top) and velocity (bottom) profiles in the highly relativistic regime.

at $t = 2.0 fm/s$ are presented in Fig. 8, which shows that for this case $\beta \sim 0.99$ and $\gamma(u) \sim 9$. This indicates that our model is numerically stable for simulating relativistic fluids with ultra-high velocities. The required CPU time for this simulation is 781 ms.

Astrophysical application

As an astrophysical application, we simulate a relativistic shock wave, generated by, say, a supernova explosion, colliding with a massive interstellar cloud, e.g. molecular gas [37]. The ejecta from the explosion of such supernovae are known to sweep the interstellar material up to relativistic velocities along the way (relativistic outflows) [38]. We perform a three-dimensional simulation of a shock wave passing through a cold spherical cloud in a lattice of $200 \times 100 \times 100$ cells. As mentioned earlier, in order to solve the equation of conservation of particle density, an extra distribution function is used, Eq.(58). As initial condition, the region is divided in two zones by the plane $x = 65$; at the left hand side ($x \leq 65$), the density is set to $n_1 = 0.6 cm^{-3}$ and the temperature to $T_1 = 10^4 K$. The massive cloud is modeled as a solid sphere with radius of 10 cells and centered at the location $(100, 50, 50)$, where we neglect the drag force

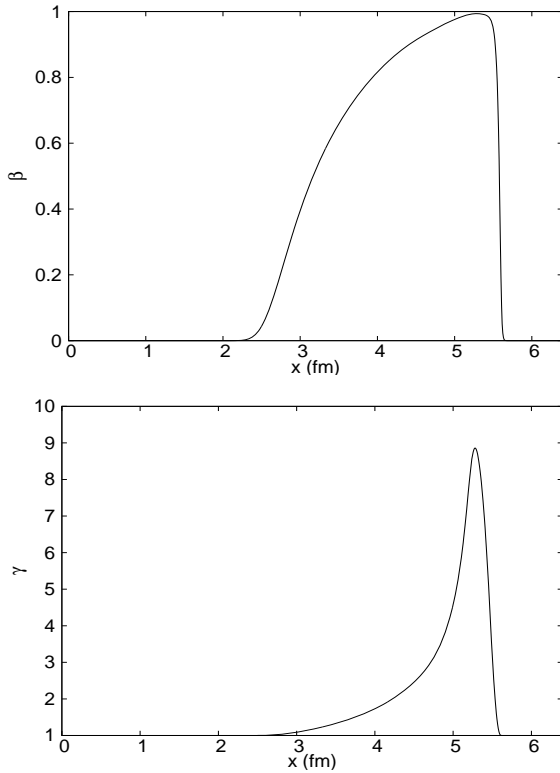


FIG. 8. Results of the simulation for the velocity profile (top) and Lorentz's factor (bottom) in the ultra-high relativistic regime.

acting on the cloud due to the flow (the sphere will remain at the same position during the whole simulation). Open boundary conditions are applied to all the external boundaries, except the left one, where an inlet boundary condition is applied by fixing the distribution function with the equilibrium distribution calculated at the initial condition, i.e. n_0 and T_0 . On the surface of the cloud, the cells evolve to the equilibrium distribution function evaluated at the constant values of $n = n_1$, $T = T_1$ and $\mathbf{u} = 0$. It should be mentioned that, at each cell, the pressure can be calculated using the relation $P = nT$.

By changing the initial condition at the right hand side of the dividing plane ($x > 65$), we are able to tune the velocity of the shock wave. Two different velocities are considered here. For the first case, we consider a shock wave at weakly relativistic regime ($\beta = 0.2$), setting $T_0 = 2.71T_1$ and $n_0 = 0.9n_1$. For the second case, highly relativistic regime ($\beta = 0.9$), these values are $T_0 = 54.77T_1$ and $n_0 = 10.95n_1$. Fig. 9 shows the results of the 3D simulation of the shock wave, after colliding with the massive interstellar cloud for the density field for both cases. The simulations are performed in the inviscid case, where $\alpha = 0.2$ and $\delta_t/\delta_x = 0.15$. The density field is plotted in logarithmic scale at $t = 1000$ time step, where red and blue denote high and low values, respectively, and streamlines represent the velocity field. In

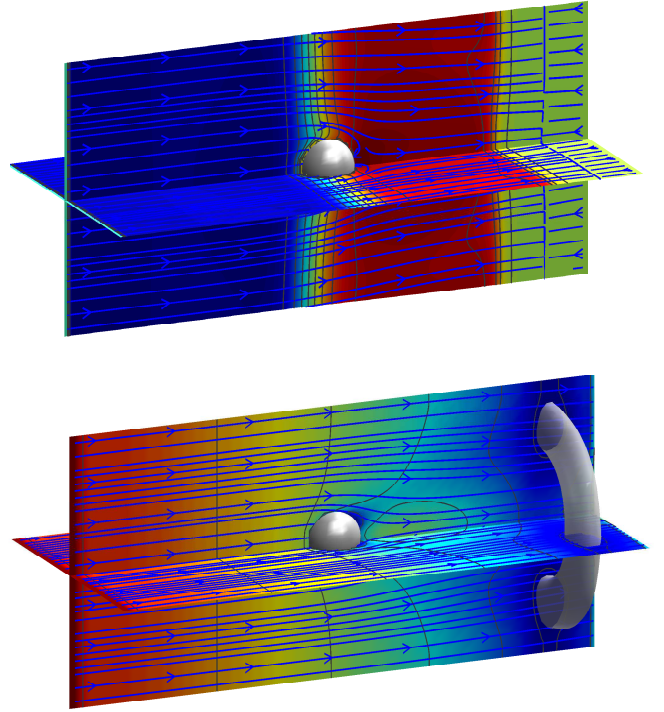


FIG. 9. Snapshots of the three-dimensional simulation of a relativistic shock wave colliding with a massive interstellar cloud. Here, the density field is plotted in logarithmic scale in the weakly relativistic regime (top) and highly relativistic regime (bottom) at time $t = 1000$. The iso-surface in the second figure illustrates a region of low density ($\log(n/n_0) \sim -2.5$).

this figure, we observe an increase in the density downstream of the collision, likely due to the fact that, during the propagation, the shock wave collects interstellar material and pushes it against the cloud (sweeping effect). However, at higher speeds, this increase on the density becomes less pronounced, and the passing of the shock wave generates a ring-shape region of low density downstream (see isosurface in Fig. 9).

In order to study the viscous effects, the same simulations are performed by introducing the dissipation and taking $\tau = 1$. Fig. 10 shows the pressure, density and temperature profiles at weakly and highly relativistic regimes for both, inviscid and viscous cases. The results are shown along the x axis at $y = z = 50$ and at $t = 600$ time steps. Note that since P_0 , n_0 , and T_0 take very different values for the weakly and highly relativistic regimes, in order to make a clear comparison of the results, we have normalized P , n , and T with P_0 , n_0 , and T_0 , respectively. As it can be appreciated, the viscous effects become relatively more important downstream of the cloud. Furthermore, it causes a pressure drop and decreases the density, while inducing a corresponding increment of temperature in the gas. Note, that the effects on the temperature are more significant at highly rela-

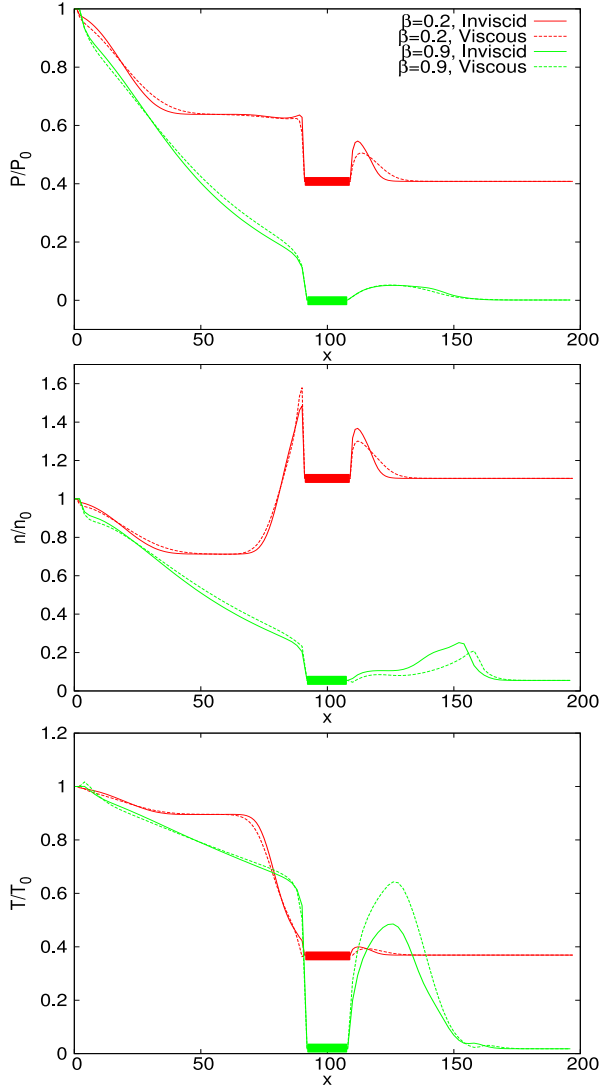


FIG. 10. Pressure (top), density (middle) and temperature (bottom) profiles in the weakly and highly relativistic regimes, for the inviscid and viscous case. The results are shown along the x axis at $y = z = 50$ at $t = 600$ time steps. The thicker lines denote the regions where the interstellar cloud is located.

tivistic regime than the pressure drop, while an opposite behavior is found at weakly relativistic regime.

IV. CONCLUSIONS

In this paper, we have introduced a relativistic lattice Boltzmann model that is able to handle relativistic fluid dynamics at very high velocities. For this purpose,

we have first expanded the Maxwell Jüttner distribution in orthogonal polynomials, by assuming as weight function the equilibrium distribution at the local rest frame. A discretization procedure has been applied in order to adjust the expansion to the D3Q19 cell configuration, which, in order to avoid a multi-time evolution of the Boltzmann equation, leads to the problem of recovering only the conservation of the momentum-energy tensor. However, in the ultra-relativistic regime ($\epsilon = 3p$) the entire dynamics of the system is governed by this equation and the first order moment is not required. To extend the model to high velocities ($\beta \sim 1$), we use a flux limiter scheme and introduce a bulk viscosity term into the Boltzmann equation, to increase the numerical stability in presence of discontinuities.

In order to validate our model, we have compared the numerical results for shock waves in viscous quark-gluon plasmas with the results of other existing models, and found very good agreement. In addition, to the best of our knowledge, we have for the first time successfully simulated shock waves in relativistic viscous flow for $\beta > 0.6$. We have also suggested a way to simulate near-inviscid flows (Euler equation) using the extended model by modifying the collision step. For this case, we have compared the results with the analytical solution, finding again very satisfactory agreement. This offers a promising strategy to study astrophysical flows at very high speeds and negligible viscous effects. Additionally, we have shown that our model is capable of simulating the Riemann problem at ultra-high relativistic flows ($\gamma \sim 10$). Finally, we have studied the collision of a shock wave colliding with a massive interstellar cloud in weakly and highly relativistic regimes, for both inviscid and viscous cases.

Summarizing, we have proposed a model which is simple, numerically efficient, and capable of simulating highly relativistic flows. It can also be used to simulate near-inviscid flows. Moreover, like other lattice Boltzmann methods, our model is highly adaptable to parallel computing and can be used to simulate complex geometries. These features make this model appealing for prospective applications in relativistic astrophysics and high energy physics. Extensions of this model to include higher order lattices so as to recover more moments of the equilibrium distribution, make a very interesting subject for future research.

ACKNOWLEDGMENTS

We acknowledge financial support from the European Research Council (ERC) Advanced Grant 319968-FlowCCS and financial support of the Eidgenössische Technische Hochschule Zürich (ETHZ) under Grant No. 0611-1.

[1] M. J. Blandford, R. D.; Rees, MNRAS **169**, 395 (1974).

[2] K. Nishihara, J. Wouchuk, C. Matsuoka, R. Ishizaki, and

V. Zhakhovsky, Philosophical Transactions of the Royal Society A: Mathematical, Physical and Engineering Sciences **368**, 1769 (2010).

[3] E. Shuryak, Progress in Particle and Nuclear Physics **53**, 273 (2004).

[4] M. Dubal, Computer Physics Communications **64**, 221 (1991).

[5] L. Hernquist and N. Katz, Astrophysical Journal Supplement Series **70**, 419 (1989).

[6] S. Siegler and H. Riffert, The Astrophysical Journal **531**, 1053 (2008).

[7] L. Wen, A. Panaiteescu, and P. Laguna, The Astrophysical Journal **486**, 919 (1997).

[8] F. Eulderink and G. Mellema, Astronomy and Astrophysics Supplement **110**, 110 (1995).

[9] J. Yang, M. Chen, I. Tsai, and J. Chang, Journal of Computational Physics **136**, 19 (1997).

[10] R. Benzi, S. Succi, and M. Vergassola, Physics Reports **222**, 145 (1992).

[11] H. Chen, S. Chen, and W. Matthaeus, Physical Review A **45**, 5339 (1992).

[12] S. Succi, *The lattice Boltzmann equation for Fluid Dynamics and Beyond* (Oxford University Press, New York, 2001).

[13] S. Succi, J. Wang, and Y.-H. Qian, International Journal of Modern Physics C **08**, 999 (1997).

[14] G. R. McNamara and G. Zanetti, Phys. Rev. Lett. **61**, 2332 (1988).

[15] F. Higuera and J. Jimenez, EPL (Europhysics Letters) **9**, 663 (2007).

[16] S. Succi, The European Physical Journal B-Condensed Matter and Complex Systems **64**, 471 (2008).

[17] X. Shan and X. He, Phys. Rev. Lett. **80**, 65 (1998).

[18] P. L. Bhatnagar, E. P. Gross, and M. Krook, Phys. Rev. **94**, 511 (1954).

[19] M. Mendoza, B. M. Boghosian, H. J. Herrmann, and S. Succi, Phys. Rev. Lett. **105**, 014502 (2010).

[20] M. Mendoza, B. M. Boghosian, H. J. Herrmann, and S. Succi, Phys. Rev. D **82**, 105008 (2010).

[21] I. Bouras, E. Molnar, H. Niemi, Z. Xu, A. El, O. Fochler, C. Greiner, and D. Rischke, Phys. Rev. Lett. **103**, 32301 (2009).

[22] Q. Li, K. H. Luo, and X. J. Li, Phys. Rev. D **86**, 085044 (2012).

[23] P. Romatschke, M. Mendoza, and S. Succi, Phys. Rev. C **84**, 034903 (2011).

[24] J. Anderson and H. Witting, Physica **74**, 466 (1974).

[25] C. Marle and C. Hebad, Seances Acad. Sci. **260**, 6539 (1965).

[26] J. Stewart, *Non-equilibrium Relativistic Kinetic Theory* (Springer, Berlin, 1971).

[27] C. Cercignani and G. Kremer, *The Relativistic Boltzmann Equation: Theory and Applications* (Birkhauser, Boston; Basel; Berlin, 2002).

[28] D. Hupp, M. Mendoza, I. Bouras, S. Succi, and H. Herrmann, Physical Review D **84**, 125015 (2011).

[29] X. Pan, A. Xu, G. Zhang, and S. Jiang, International Journal of Modern Physics C **18**, 1747 (2007).

[30] P. Dellar, Physical Review E **64**, 031203 (2001).

[31] P. Romatschke, International Journal of Modern Physics E **19**, 1 (2010).

[32] M. Mendoza, I. Karlin, S. Succi, and H. Herrmann, arXiv:1301.3420 to appear in JSTAT (2013).

[33] R. Mei and W. Shyy, Journal of Computational Physics **143**, 426 (1998).

[34] D. H. Rischke, S. Bernard, and J. A. Maruhn, Nuclear Physics A **595**, 346 (1995).

[35] K. Thompson, Journal of Fluid Mechanics **171**, 365 (1986).

[36] B. Nadiga, Journal of statistical physics **81**, 129 (1995).

[37] C. McKee and B. Draine, Science **252**, 397 (1991).

[38] A. M. Soderberg *et al.*, Nature Letters **463**, 513 (2010).